Journal of Molecular Liquids 344 (2021) 117775

Contents lists available at ScienceDirect

Journal of Molecular Liquids

journal homepage: www.elsevier.com/locate/molliq

Static structure, collective dynamics and transport coefficients in the liquid Li-Pb alloy. An *ab initio* molecular dynamics study

M.M.G. Alemany [a], Jaime Souto-Casares [a], Luis E. González [b,*], David J. González [b]

[a] Departamento de Física de Partículas, Área de Física de la Materia Condensada, Facultad de Física, Universidad de Santiago de Compostela, E-15706 Santiago de Compostela, Spain
[b] Departamento de Física Teórica, Átomica y Óptica, Facultad de Ciencias, Universidad de Valladolid, E-47011 Valladolid, Spain

ARTICLE INFO

Article history:
Received 16 August 2021
Revised 1 October 2021
Accepted 3 October 2021
Available online 9 October 2021

Keywords:
Liquid Li-Pb alloy
Structure and dynamics
Ab initio simulations

ABSTRACT

Several static and dynamic properties of the liquid Li-Pb alloy at diverse compositions, have been calculated by means of *ab initio* molecular dynamics simulation study. This alloy has attracted much attention because of the finding of fast sound at the $Li_{0.80}Pb_{0.20}$ composition and also the technological interest of the the eutectic composition, $Li_{0.17}Pb_{0.83}$, as a component of the blanket in fusion reactors.

Results are reported for total static structure factors, which are compared with the available experimental data. An additional analysis of the structure allows the quantification of the heterocoordinating tendencies in this alloy, which at the $Li_{0.80}Pb_{0.20}$ composition are largest and lead to a Pb-centered polyhedral structure, where, however, Li_4Pb units are not present.

Regarding the collective dynamics, the calculated partial dynamic structure factors exhibit side peaks indicative of propagating density fluctuations, including density fluctuation modes with phase velocity greater than the hydrodynamic sound velocity. Also, the longitudinal and transverse dispersion relations have been calculated and its different branches analysed. We find all the high frequency branches to behave as optic-like modes, contrary to other interpretations in terms of an acoustic-like fast sound mode.

Some transport coefficients such as self- and inter-diffusion coefficients, shear viscosities and adiabatic sound velocities, have also been calculated. Finally, the obtained results for the electronic density of states clearly indicate the metallic character of the liquid Li_xPb_{1-x} alloy.

1. Introduction

In the last four decades, liquid binary mixtures have been extensively investigated, both experimentally and by computer simulations, with the main aim focused towards understanding the microscopic mechanisms behind the collective excitations and the interdifussion processes. In this context, special attention has been devoted to those binary mixtures composed of particles with disparate masses because of the appearance of a high frequency mode with a phase velocity much greater than the value predicted by an extension of the hydrodynamic sound to large wavevectors. This has been the case in studies performed for $Li_{0.80}Pb_{0.20}$, $Na_{0.50}Cs_{0.50}$ and $Li_{0.30}Bi_{0.70}$ using Molecular Dynamics (MD) simulations [1–4] and inelastic neutron scattering (INS) experiments [5–8].

In fact, kinetic theory calculations for binary mixtures with large atomic mass difference [2], have found that this high frequency mode was supported by the light atoms only and if the associated high frequency were interpreted in terms of a phase velocity of a propagating acoustic mode (also called "fast sound") it would lead to phase velocities characteristic of the pure (light) component. Moreover, calculations using the revised Enskog theory (RET) [9] for binary hard sphere mixtures predicted, besides the hydrodynamic sound, two propagating collective modes. One was identified with the fast sound whereas the other, with an associated phase velocity smaller than the hydrodynamic one, was named "slow sound".

However, the very nature of this new high frequency excitation still remains a controversial point with differing opinions concerning it low q behaviour. Thus, it has been suggested that as $q \to 0$ this new mode would merge into the hydrodynamic sound of the mixture whereas other authors have identified it with an optic-like mode that would take a non-zero frequency value as q goes into the long-wavelength region.

Molten $Li_{0.80}Pb_{0.20}$ has been the system where this high frequency excitation has been more closely scrutinized. A first study was performed by Jacucci et al. [1] who carried out a classical

* Corresponding author.
E-mail address: luisen@metodos.fam.cie.uva.es (L.E. González).

https://doi.org/10.1016/j.molliq.2021.117775
0167-7322/

molecular dynamics (CMD) simulation for the liquid $Li_{0.80}Pb_{0.20}$ alloy at T = 1085 K. The liquid alloy was modelled as a mixture of positive Li and negative Pb ions and the interactions among the ions were represented by interatomic pair potentials consisting of a hard core repulsion plus a screened Coulomb interaction. They found that the Li-Li partial dynamic structure factor, $S_{LiLi}(q,\omega)$, displayed a high-frequency side peak, which dispersed linearly with a velocity ($\approx$ 7500 m/s) which is substantially greater than the hydrodynamic sound velocity of the mixture ($c_s \approx 2000$ m/s). This feature was explained as a collective excitation supported by the light atoms and it was named the "fast sound" mode.

Shortly after, additional INS experiments [6,7] on the liquid $Li_{0.80}Pb_{0.20}$ alloy were performed in search of excitations with frequencies well above that of hydrodynamic sound. The obtained data confirmed the existence of a high-frequency mode supported by the light component (Li atoms) only, although its velocity ($\approx$ 4500 m/s) was clearly smaller than the "fast sound" suggested by the previous CMD simulations [1]; in fact, this new estimate for the velocity was comparable to that of pure Li at similar thermodynamic conditions of number density and temperature. Moreover, the INS data of Alvarez et al. [7] suggested that this high frequency mode had features which clearly deviated from those expected for the propagation of a sound wave and pointed to the presence of rather localized, out-of-phase atomic motions, resembling those exhibited by Coulomb systems [10]. Actually, some theoretical models (viscoelastic model [4], generalized collective modes (GCM) theory [11]) envisage that a specific fast sound "mode" is not strictly necessary to account for the presence of a side peak in the partial dynamic structure factor of the light species. It may also appear as a consequence of a weighted sum of an "extended sound mode", which goes into the hydrodynamic sound in the long-wavelength limit, and a kinetic (non-hydrodynamic) mode of much higher frequency which goes to a non-zero frequency for $q \to 0$ and whose weight in the sum decreases towards zero for decreasing wavevectors.

Fernandez-Perea et al. [3] have also performed CMD simulations for the liquid $Li_{0.80}Pb_{0.20}$ alloy by using the same interatomic pair potentials as Jacucci et al. [1]. However, their simulation box contained 6720 particles which allowed reaching q-values as small as 0.019 $Å^{-1}$ and therefore to gather information well into the hydrodynamic region. Oddly enough, in constrast to the conclusions from the INS data of Alvarez et al. [7], their results showed the existence of two branches of collective excitations which merged, for $q \leqslant 0.11$ $Å^{-1}$ into the usual hydrodynamic linear dispersion.

Bryk and Mryglod [12] have also studied the static and dynamic properties of the liquid $Li_{0.80}Pb_{0.20}$ alloy by combining CMD simulations (with the same pair potentials as in Ref.[1,3]) with the generalized collective modes (GCM) method. Basically, the time correlation functions yielded by the CMD simulations are analyzed within the framework of the GCM method which provides some additional insight into the hydrodynamic and non-hydrodynamic collective processes existing in the liquid with different spatial and time scales. Their results showed the existence of two branches of collective excitations which in the hydrodynamic limit were associated to hydrodynamic sound and optic-like excitations respectively.

Interestingly, previous to the above mentioned developments associated with the liquid $Li_{0.80}Pb_{0.20}$ alloy, the liquid Li-Pb alloy had already attracted much experimental and theoretical work. On the experimental side, we notice that most measured properties show a non-ideal dependence with composition and the maximum deviation from ideal behaviour is usually found around the composition, $Li_{0.80}Pb_{0.20}$. For instance, at this composition the stability function has a marked peak (suggesting strongly reduced concentration fluctuations) [13], the entropy of mixing shows a dip [14], the excess volume per atom has a maximum relative deviation of about −18% [15], the interdiffusion coefficient shows a maximum [16] and the electrical resistivity attains a maximum value of $\approx$ 500 $\mu\Omega$ cm, although the system still remains metallic [17]. It is believed that this behaviour is related to the existence of some electronic charge transfer from the Li atoms to the Pb atoms which is driven by the significant electronegativity difference between both type of atoms with a net effect of rendering the bond partially ionic. In fact, several studies showed that some of the thermodynamic [18,19], electronic [20], structural [21], and dynamic [16,22] properties of $Li_{0.80}Pb_{0.20}$ could be at least qualitatively explained by assuming the existence, even if transient, of Li_4Pb units in the melt. On the other hand, the static structure of the liquid Li-Pb alloy has been determined, for several temperatures and concentrations, by means of neutron scattering (NS) experiments [23,24]; moreover, the subsequent analysis pointed out to the existence of heterocoordinating tendencies which become more marked near the $Li_{0.80}Pb_{0.20}$ composition.

As for the dynamical properties, we mention that the first INS experiment was performed by Soltwisch et al. [25,22] for the liquid $Li_{0.80}Pb_{0.20}$ alloy at T = 1023, 1098 and 1173 K. These experiments yielded the quasielastic part of the concentration-concentration Bathia-Thornton dynamic structure factor, $S_{cc}(q,\omega)$. This is so because if the ^{7}Li isotope is used in the alloy, then the coherent part of the scattered intensity (which depends on the momentum transfer, q, and energy transfer, $\hbar\omega$) is proportional to $S_{cc}(q,\omega)$. Moreover, as the incoherent contribution is dominated by the ^{7}Li atoms, the analysis of the data was performed by fitting the measured total scattered intensity to a sum of a term proportional to the $S_{cc}(q,\omega)$ plus another one proportional to the incoherent contribution of the ^{7}Li atoms. By restricting the analysis to the quasi-elastic region and performing a fitting to the analytical hydrodynamic limits of both contributions, they obtained estimates of the interdiffusion and self-diffusion coefficients in this alloy.

Although the liquid Li-Pb alloy has been intensively studied by means of MD simulations, specially after the detection of the high frequency mode, however it is startling that *ab initio* MD (AIMD) simulation studies of its dynamical properties are yet to be performed. Moreover, all previous CMD simulation studies have been carried out using exactly the same interatomic pair potentials, i.e. hard core plus screened Coulomb interaction. There have been, in fact, a few studies that used effective manybody embedded atom model potentials, that either did not [26], or did [27], include also screened Coulomb potentials between the components, but they did not delve into the analysis of dynamic properties. Therefore, it seems important to perform a study where the interactions among the atoms/ions are evaluated at a more fundamental level. To our knowledge, the only AIMD study of this alloy [28] was focused on two concentrations, namely $Li_{0.50}Pb_{0.50}$ and $Li_{0.80}Pb_{0.20}$, and they reported results for static and electronic properties only.

This paper describes an AIMD simulation study of the structural, dynamical and electronic properties of the liquid Li_xPb_{1-x} alloy at several concentrations. Obviously, we have considered the $Li_{0.80}Pb_{0.20}$ composition as we are interested in attaining a more detailled picture of its collective excitations by analysing magnitudes which are not yielded by experiment. Another interesting alloy is the eutectic composition, $Li_{0.17}Pb_{0.83}$, which due to its low melting point, high boiling point and appropriate absorption and activation cross section for neutrons has been proposed [29] as a blanket in nuclear fusion reactors. Moroever, it has the capability of acting as a tritium breeder and neutron multiplier and it could also be used as a coolant. Therefore, it is important to gather as much information as posible concerning the properties of the

eutectic alloy. Finally, we have also studied two other concentrations for which some experimental data are available. In this way, it will be possible to analyze the way in which the various properties are influenced by the composition.

The present AIMD simulations have been performed by using the PARSEC code [30] which has already been used to study some pure liquid metals [31–33] (including liquid Pb near its triple point) and alloys [34], as well as other types of liquids and glasses [35]. Nevertheless, the complex nature of the liquid Li_xPb_{1-x} alloy poses a stringent test on the capability of this method to describe this type of systems. Computational details are briefly described in Section 2, and in Section 3 we present and discuss our results, comparing them with available experimental data. Finally, in Section 4, we summarize our main conclusions.

2. Technical details

Within the PARSEC method [30], the Density Functional Theory-based Kohn–Sham equations [36,37] were solved self-consistently on a rectangular three-dimensional real-space grid within a supercell geometry [38]. The core electrons of the Li and Pb atoms were represented by Troullier-Martins norm-conserving pseudopotentials [39], generated for the reference configurations $[He]2s^12p^0$ and $[Xe](4f^{14}5d^{10})6s^26p^26d^05f^0$, respectively, and with associated radial cutoffs of 2.8 a.u. and 3.2 a.u. The potentials were made separable by the procedure of Kleinman and Bylander [40], applied in real space, with the p potential chosen to be the local component. A partial-core correction for nonlinear exchange correlation was included for Pb. The local density functional of Ceperley and Alder [41], as parametrized by Perdew and Zunger [42], was used and the single Γ-point was employed in sampling the Brillouin zone. A spacing of 0.64 a.u. was used for constructing the real-space grid.

Calculations were performed for the thermodynamic states shown in Table 1. The total number of atoms considered in the simulation varied from 240 (for x_{Li} = 0.50) to 330 atoms (for x_{Li} = 0.80) and the simulation was started by placing the atoms, at random, in a cubic supercell with dimensions chosen so as to obtain the respective experimental number density [15]. The temperatures of the simulations were chosen as those of (or close to) the corresponding NS experiments. The AIMD simulation runs were performed with the ionic dynamics being generated using the Beeman algorithm [43] with Hellmann–Feynman forces [44]. After thermalization, the number of time steps that were used for calculating the static, dynamic and electronic properties reported below varied from 20000 (80 ps of simulation time for $Li_{0.80}Pb_{0.20}$) to 28000 (112 ps of simulation time for $Li_{0.17}Pb_{0.83}$).

3. Results and discussion

3.1. Structural properties

Fig. 1 shows the calculated partial pair distribution functions $g_{ij}(r)$ of the liquid Li_xPb_{1-x} alloy at four concentrations. We observe that the main peak's height of the $g_{LiPb}(r)$ is always similar (x_{Li} = 0.17) or higher than those of the $g_{LiLi}(r)$ and $g_{PbPb}(r)$. This feature is indicative of heterocoordinating tendencies in the alloy and implies that each atom tends to be surrounded, in its first coordination shell, by atoms of the other species. Notice that when x_{Li} = 0.80, the main peak in $g_{PbPb}(r)$ has practically vanished and the second peak is unusually high. This confirms the results of the pioneering AIMD study of Senda et al. [28], although with increased statistical accuracy. In that study some similarity between the structure of the liquid $Li_{0.80}Pb_{0.20}$ alloy and that of the crystalline compound Li_7Pb_2 (with similar composition, $x_{Li} \approx 0.78$) was highlighted, including the lack of Pb atoms as near neighbors of a Pb atom, and the long Pb-Pb distance, which is somewhat smaller in the solid (4.75 $Å^{-1}$) than in the liquid, where the maximun of $g_{PbPb}(r)$ is located around 5.2 $Å^{-1}$. There is another solid compound in the phase diagram of the alloy, which is the Li-richest one, that after several revisions has been assigned as $Li_{17}Pb_4$ [45] with a composition ($x_{Li} \approx 0.81$) even closer to the liquid one studied. Its atomic structure is rather complex, with 105 atoms in the primitive unit cell, and can be studied as composed of two $Li_{20}Pb_6$ clusters, one $Li_{22}Pb_4$ cluster and one $Li_{23}Pb_4$ cluster. If full charge transfer is assumed from Li (becoming Li^+) to Pb (becoming Pb^{4-}) the first two clusters would have negative charge (−4) while the latter two would instead be positively charged (+6 and +7, respectively). Consequently some more electron charge must be localized outside the clusters (nominally 5 electrons) and in fact this is what has been found in a recent *ab initio* study of this solid compound [46], which therefore qualifies as an electride. In fact the charge transfer was found not to be complete but partial, so that the clusters retained the sign but not the magnitude of the charges, and the total number of electrons outside the clusters was indeed smaller and localized in 4 particular regions of the structure (see [46] for details). Alternatively, the atomic structure can be described as built from different types of Pb centered Li polyhedra [46]. Three of these building blocks contain 13 Li atoms while the fourth has 14 of them. Therefore, the average number of Li atoms around a Pb in the solid is 13.25, there are no Pb near neighbors of a Pb atom and the Pb-Pb distances are again quite long, in fact distributed within a range from approximately 4.75 to 5.50 Å [46]. Consequently, the liquid structure shares even more similarities with that of the $Li_{17}Pb_4$ compound. Such polyhedral arrangements are common in other types of solid compounds, like oxides, and there is some consensus that the molten structures can also be described in terms of polyhedra, although distorted or even with changes in the number of faces of the polyhedra [47]. We will later analyze this possibility for the particular case of liquid $Li_{0.80}Pb_{0.20}$ below.

From the $g_{ij}(r)$, we can obtain the coordination numbers n_{ij} describing the number of j-type particles around an i-type particle within a sphere of radius R_{ij}, i.e.

$$n_{ij} = 4\pi\rho\, x_j \int_0^{R_{ij}} r^2 g_{ij}(r) dr, \quad (1)$$

where R_{ij} is usually identified [48] with the position of the first minimum of the related partial radial distribution function, $4\pi r^2 g_{ij}(r)$. A quantitative estimate of the short range order (SRO) in the alloy and

Table 1
Thermodynamic input data of the liquid Li_xPb_{1-x} alloy used in the present AIMD simulation study. The total ionic number density, ρ, was taken from [15].

x_{Li}	ρ ($Å^{-3}$)	T(K)
0.17	0.0325	775
0.50	0.0390	775
0.62	0.0431	775
0.80	0.0436	1075

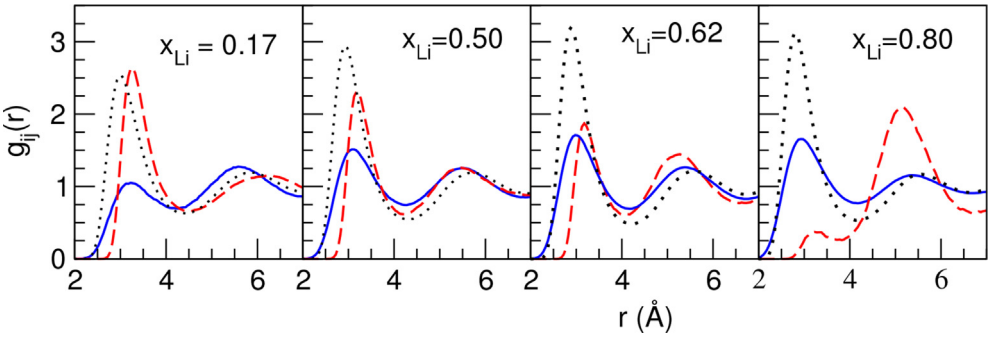

Fig. 1. Partial pair distribution functions $g_{ij}(r)$ of the liquid Li_xPb_{1-x} alloy at x = 0.17, 0.50, 0.62 and 0.80. Full blue, dashed red and dotted lines correspond to $g_{LiLi}(r), g_{PbPb}(r)$ and $g_{LiPb}(r)$, respectively.

its dependence with concentration is provided by the Warren [49] SRO parameter for the first neighbour shell, α_1. It is defined as

$$\alpha_1 = 1 - \frac{n_{ij}}{x_j(x_i n_j + x_j n_i)} (j \neq i = 1, 2) \quad (2)$$

where x_j is the concentration of the j-type particles and $n_i = n_{ii} + n_{ij}$ (i,j = 1, 2). The computed values of n_{ij} and α_1 are given in Table 2 where its is observed that α_1 takes negative values for all concentrations; this feature points to heterocoordinating tendencies in the alloy, which for the concentrations studied in this work are most marked in the case of $x_{Li} = 0.80$.

Note also that the average number of Li atoms around a Pb atom in the alloy with $x_{Li} = 0.80$ is around 11, which is substantially smaller than what was found in solid $Li_{17}Pb_4$, pointing to an important change in the characteristics of the Li polyhedra around a Pb atom, if this picture is at all correct.

In order to check if the polyhedral description of the liquid structure in $Li_{0.80}Pb_{0.20}$ is a valid one (results are shown in figure 2) we have analyzed all of the configurations generated in the following way. For each Pb atom we have identified those Li atoms that are its near neighbors. Then we have checked if any of the other Pb atoms lies inside the convex hull of the set of these Li atoms, i.e. inside the polyhedron whose vertices are the Li atoms. In order to perform this check we have used a simplified version of the GJK (Gilbert-Johnson-Keerthi) algorithm, which is widely used to detect collisions of 2- or 3-dimensional objects in visualization programs. If the polyhedral description of the liquid were correct then no such cases should occur, as each Pb atom should be inside its own polyhedron.

Note that this question is not just a simple comparison about some Pb-Pb distances being shorter than Pb-Li distances, which certainly happens as evidenced by the small, but not null, first peak of $g_{PbPb}(r)$ that lies within the first peak of $g_{PbLi}(r)$. The problem is strictly a 3-dimensional geometric one: for example, the distance between the centers of two face-sharing regular tetrahedra is smaller than the distance between the center and the vertex of the tetrahedra.

As a result of the check we have found that out of the 20000 configurations generated only in two of them there was just a single Pb atom that was inside the polyhedron associated to a different Pb atom. Therefore we can confidently say that the polyhedral picture is not perfect, but almost so.

The average number of Li atoms that are near neighbors of a Pb atom, as already indicated above, is around 11. However, the number of Li atoms in the polyhedra are of course distributed, and Fig. 2 shows this distribution. We see the appearance of $PbLi_7$ to $PbLi_{15}$ polyhedra, with $PbLi_{11}$ being the most abundant one. Since the average concentration in the alloy implies 4 Li atoms per Pb atom, obviously there must be many Li atoms shared by more than one Pb atoms, i.e. Li atoms that belong to the polyhedra of several Pb atoms. But what can be definitely discarded is the presence of Li_4Pb units that have been suggested by other authors to exist in order to justify the properties of the alloy at this particular composition [16,18–22].

In order to compare our AIMD results with the NS data of Ruppersberg and Reiter [23,24], we have first calculated the Ashcroft-Langreth (AL) partial static structure factors $S_{ij}(q)$ which are depicted in Fig. 3. The $S_{LiLi}(q)$ show a prepeak whose position moves from $q \approx 1.5$ Å^{-1} (for $x_{Li} = 0.17$) to $q \approx 1.65$ Å^{-1} (for $x_{Li} = 0.80$); moreover it also shows another peak at $q \approx 2.45$ Å^{-1} (for $x_{Li} = 0.17$) whose amplitude grows with increasing Li concentration so that it becomes its main peak while its position slightly moves to $q \approx 2.55$ Å^{-1} (for $x_{Li} = 0.80$). Remarkably, the prepeak exhibited by $S_{LiLi}(q)$ at $x_{Li} = 0.80$ had not been predicted by previous CMD simulations [1,4,3]. The $S_{PbPb}(q)$ has for $x_{Li} = 0.17$ a main maximum at $q \approx 2.35$ Å^{-1}, which for increasing Li concentration diminishes its amplitude while, at the same time, another peak develops at a smaller q ($q \approx 1.6$ Å^{-1}) so that for $x_{Li} = 0.80$ has become the main peak. Note also that the position of the first peak or prepeak in the $S_{LiLi}(q)$ and $S_{PbPb}(q)$ are almost coincident with the position of the first minimum of $S_{LiPb}(q)$, which is another indication of a certain amount of chemical ordering.

This type of ordering is clearly revealed in the Bhatia-Thornton (BT) partial structure factors [50–53] that we have also evaluated and are shown in Fig. 4, namely the number-number, $S_{NN}(q)$, the concentration-concentration, $S_{CC}(q)$, and the number-concentration, $S_{NC}(q)$, partial structure factors. Their long-wavelength limits provide microscopic information on the ordering tendencies of the liquid alloy, in particular $S_{CC}(q \to 0)$, for which we have obtained the following results: $S_{CC}(q \to 0)/(x_{Li}x_{Pb})$

Table 2
Calculated coordination numbers n_{ij} and the Warren-Cowley short-range order parameters $\alpha_1^{(i)}$ for the liquid Li_xPb_{1-x} alloy at the thermodynamic states given in Table 1.

x_{Li}	n_{LiLi}	n_{LiPb}	n_{PbPb}	n_{PbLi}	α_1
0.17	0.8	9.2	9.2	1.9	−0.09
0.50	4.6	6.6	5.0	6.6	−0.16
0.62	6.5	5.3	3.2	8.7	−0.18
0.80	8.0	2.8	0.3	10.9	−0.26

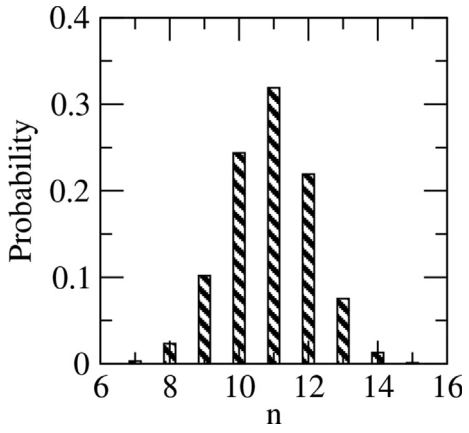

Fig. 2. Distribution of $PbLi_n$ polyhedra present in the $Li_{0.80}Pb_{0.20}$ alloy.

$\approx$ 0.40, 0.35, 0.32 and 0.10 ($\pm$ 20%) at x_{Li}= 0.17, 0.50, 0.62 and 0.80, respectively. These estimates are smaller than unity, which clearly suggests heterocoordination tendencies, in agreement with the information provided by the Warren-Cowley SRO parameter. For all concentrations, $S_{CC}(q)$ shows a distinct main peak at around $q \approx 1.6$ Å^{-1}, which coincides with the positions of the first peak/prepeak in $S_{LiLi}(q)$ and $S_{PbPb}(q)$ and minimum in $S_{LiPb}(q)$, pointing thus to their physical origin as due to chemical order.

The total neutron weighted structure factor $S_T(q)$ is readily evaluated either from the AL or the BT partial structure factor. The expression for the latter case is

$$S_T(q) = \Big[(x_{Li}b_{Li} + x_{Pb}b_{Pb})^2 S_{NN}(q) + (x_{Li}b_{Li} + x_{Pb}b_{Pb})(b_{Pb} - b_{Li})S_{NC}(q) + (b_{Pb} - b_{Li})^2 S_{CC}(q)\Big]\Big[x_{Li}b_{Li}^2 + x_{Pb}b_{Pb}^2\Big]^{-1}, \quad (3)$$

where b_{Li} and b_{Pb} denote the neutron scattering lengths of Li and Pb, respectively [54]. We recall that the liquid alloy samples for the NS measurements were prepared [23,24] from the ^{7}Li isotope and natural Pb; therefore, our evaluation of the $S_T(q)$ has been made using the associated values b_{Li}= −2.22 fm and b_{Pb}= 9.40 fm.

In the case of $x_{Li} = 0.80$, due to the particular values of the scattering lengths, we have that $x_{Li}b_{Li} + x_{Pb}b_{Pb} \approx 0$, and then $S_{CC}(q) \approx x_{Li}x_{Pb}S_T(q)$, so that it can be probed by a single NS experiment. Fig. 4 shows the calculated $S_T(q)$ of the liquid Li_xPb_{1-x} alloy along with the available NS data at $x_{Li} = 0.17, 0.50, 0.62$ and 0.80 [23,24]. Notice that the shape of the experimental $S_T(q)$ undergoes significant changes as the Li concentration is increased, with its main peak moving to smaller q-values and its position being practically determined by that of the $S_{PbPb}(q)$. Nevertheless, despite those changes undergone by the $S_T(q)$, we highlight the excellent agreement with experiment achieved by the present AIMD calculations.

3.2. Dynamic properties

3.2.1. Self- and inter-diffusion

The long-time behaviour of the motion of one particle in a liquid system is characterized by the self-diffusion coefficient, and in a binary alloy two different self-diffusion coefficients exist, one for each component, D_1 and D_2. Additionally, in the case of mixtures one can consider the motion of the center of mass of the particles of each component, and the long time behaviour of the relative motion of the center of mass of particles of type 2 with respect to that of particles of type 1 comes characterized by the relative difussion coefficient, D_{12}. In an ideal mixture in which all components are identical, the relative diffusion coefficient can be expressed directly in terms of the self-diffusion coefficients of each component, through the so called ideal formula $D_{12}^0 = x_2 D_1^s + x_1 D_2^s$. Any deviation from this rule is usually reported in terms of the quantity γ_{12}, defined so that

$$D_{12} = D_{12}^0(1 + \gamma_{12}) = D_{12}^0 + x_1 x_2 D_{12}^d,$$

where we have also defined the "distinct" part of the relative diffusion coefficient, D_{12}^d. As its name suggests, it is a meassure of the influence of distinct particles, irrespective of their being of the same type or of different type, on the relative diffusion coefficient.

In computer simulations all these diffusion coefficients can be obtained as time integrals of the corresponding velocity autocorrelation functions, namely, D_i^s from $Z_i^s(t)$, which is the usual velocity autocorrelation function of a tagged i-type particle of the fluid, D_{12}^0 from $Z_{12}^0(t)$, the ideal (also called self-) relative velocity autocorrelation function, given as $Z_{12}^0(t) = x_2 Z_1^s(t) + x_1 Z_2^s(t)$, and D_{12} from $Z_{12}(t)$, the relative velocity autocorrelation function, defined as the time autocorrelation function of the relative velocity of the center of mass of particles of type 2 with respect to that of particles of type 1. Finally, D_{12}^d is obtained as the time integral of the distinct relative velocity autocorrelation function, $Z_{12}^d(t)$, defined so that

$$Z_{12}(t) = Z_{12}^0(t) + x_1 x_2 Z_{12}^d(t). \quad (5)$$

The sign of γ_{12} hints towards a dynamic tendency to homocoordination or heterocoordination, namely, if $\gamma_{12} > 0$ then particles of the same species have a greater tendency to diffuse together than particles of different species, and conversely in the case of $\gamma_{12} < 0$. More details can be found in [55]. Finally, the interdiffusion coeffi-

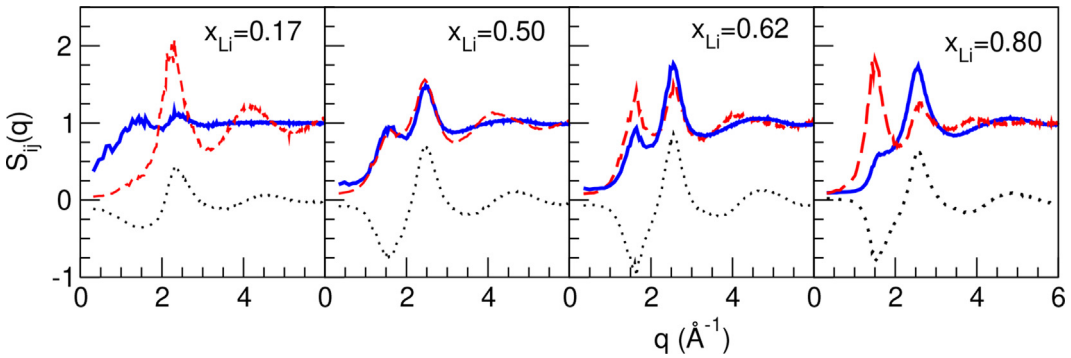

Fig. 3. Ashcroft-Langreth partial static structure factors $S_{ij}(q)$ of the liquid Li_xPb_{1-x} alloy at x_{Li} = 0.17, 0.50, 0.62 and 0.80. Full blue, dashed red and dotted lines correspond to $S_{LiLi}(q), S_{PbPb}(q)$ and $S_{LiPb}(q)$, respectively.

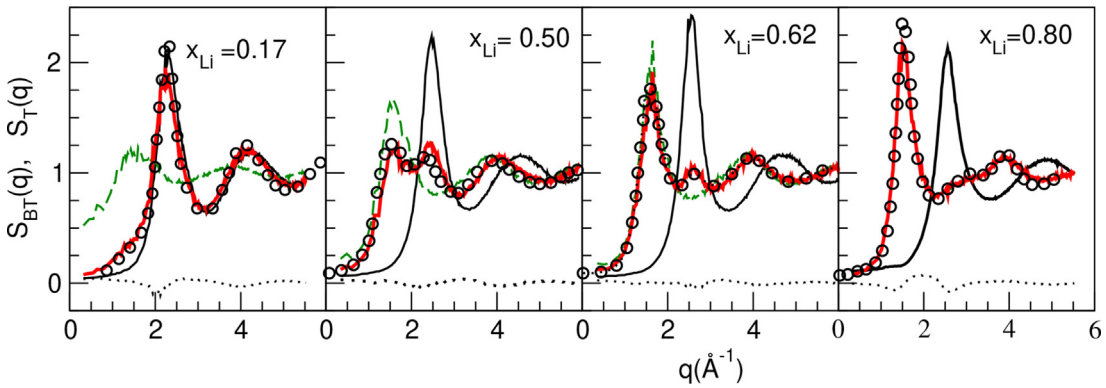

Fig. 4. Bhatia-Thornton partial static structure factors and total structure factor of the liquid Li_xPb_{1-x} alloy at x_{Li} = 0.17, 0.50, 0.62 and 0.80. Continuous, dotted and green dashed lines correspond to $S_{NN}(q), S_{NC}(q)$ and $S_{CC}(q)/(x_{Li}x_{Pb})$ respectively. The red continuous lines stand for the calculated $S_T(q)$, whereas the open circles are the corresponding NS data of Ruppersberg et al. [23,24]. Note that for $x_{Li} = 0.80$ $S_{CC}(q)/(x_{Li}x_{Pb})$ practically coincides with $S_T(q)$.

cient is given as $D_{int} = \theta D_{12}$, where $\theta = x_1x_2/S_{CC}(q \to 0)$. For a nearly ideal mixture, $\theta \approx 1, \gamma_{12} \approx 0$ and, therefore, $D_{int} \approx D^0_{12}$, which is also called Darken's approximation.

Fig. 5 shows the results obtained for the normalized self and relative VCFs. The self VCF of the heavier particles, $Z^s_{Pb}(t)$, has the slower decay and smaller backscattering because of the velocity persistence of the heavy atoms when colliding with the lighter ones. However, when the amount of Li decreases (greater proportion of heavy atoms), $Z^s_{Pb}(t)$ becomes narrower and shallower. On the other hand, $Z^s_{Li}(t)$ has a steep decay and a marked backscattering which is more pronounced with increasing concentration of Pb ions. The calculated diffusion coefficients are given in Table 3. Notice that the D^s_{Li} is always greater than D^s_{Pb} because of the smaller mass of the Li atoms. Experimental estimates for the self-diffusion coefficients are only available for the liquid $Li_{0.80}Pb_{0.20}$ alloy. Soltwisch et al. [25] fitted their measured INS data to a model that allowed to discriminate the incoherent quasielastic scattering contribution (which is dominated by ^{7}Li) and, by assuming an hydrodynamic aproximation, they obtained (for T = 1098 K) the following "experimental" estimates: D^s_{Li} = 2.13 ± 0.18 and D^s_{Pb} = 0.33 ± 0.03 (in 10^{-4}cm^2/s units), to be compared with the present AIMD values of 1.64 and 0.45 respectively (see Table 3). As for the other concentrations, we are not aware of any other experimental data; nevertheless we stress that the application of this same AIMD method to other liquid metals, including liquid Pb near melting [31,32], has yielded estimates for the self-diffusion coefficients in very good agreement with the experimental data. As for the γ_{LiPb}, we obtain negative values (suggesting mild heterocoordinating tendencies) except for the $x_{Li} = 0.80$ concentration when a positive value is obtained. Such behavior at this concentration hints towards a transient persistance of the aforementioned Li polyhedra that would surround a Pb atom, since this would imply a collective displacement of at least several of the Li atoms of the polyhedron so that like particles tend to move together. The values of γ_{LiPb}, combined with those of θ, which range from 2.5 to 10 for the concentrations considered, lead to interdiffusion coefficients that are also shown in Table 3. Here we observe a distinct deviation from the ideal mixture values, D^0_{LiPb}. The ratio D_{int}/D^0_{LiPb} takes a value around two for the $x_{Li} = 0.17, 0.50$ and 0.62 concentrations, where the relatively high values of θ overcome the negative γ_{LiPb}, but it grows to a factor of fifteen when $x_{Li} = 0.80$, where both γ_{LiPb} and θ push up the value of D_{int}. The interdiffusion coefficient in the liquid Li-Pb alloys has been measured for a range of concentrations and temperatures [16] and those values have also been included in Table 3. It is observed that the present AIMD calculations show a good agreement with experiment, including the substantial increase for $x_{Li} = 0.80$.

3.2.2. Collective dynamics

The AL and the BT partial intermediate scattering functions (ISF), $F_{ij}(q,t)$, and their Fourier transforms, the AL and BT partial dynamic structure factors, $S_{ij}(q,\omega)$, describe the collective dynamics of the fluctuations in the partial densities, component-wise in the case of the AL functions, topological and chemical in the case of the BT ones (see Ref. [34] for more details).

As a consequence of the continuity equation, that relates time derivatives of the densities with longitudinal currents, the dynamic structure factors are directly related to the Fourier transforms of

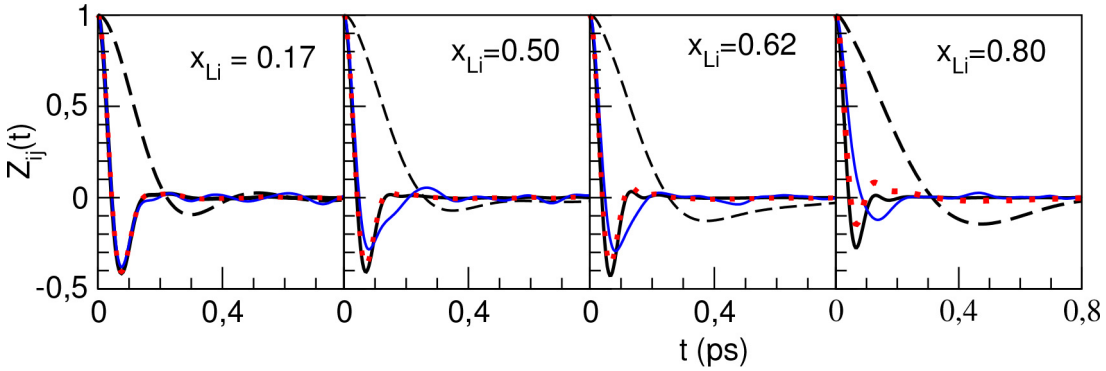

Fig. 5. Normalized self, relative and ideal VACFs for the liquid Li_xPb_{1-x} alloy at several x_{Li} values. Full, dashed, thin (blue) and dotted (red) lines correspond to $Z^s_{Li}(t), Z^s_{Pb}(t)$, $Z_{LiPb}(t)$, and $Z^0_{LiPb}(t)$, respectively.

Table 3
Diffusion coefficients (in 10^{-4}cm^2/s) and parameter γ_{LiPb} of the liquid Li_xPb_{1-x} alloy at the thermodynamicstates given in Table 1. The numbers in parenthesis are the experimental values for D_{int} obtained by Khairulin et al. [16].

x_{Li}	0.17	0.50	0.62	0.80
D^s_{Li}	0.52	0.53	0.49	1.64
D^s_{Pb}	0.33	0.33	0.26	0.45
D_{LiPb}	0.44	0.37	0.25	0.97
D^0_{LiPb}	0.49	0.43	0.35	0.69
D^d_{LiPb}	−0.35	−0.21	−0.43	1.77
γ_{LiPb}	−0.10	−0.12	−0.29	0.41
$S_{\mathrm{CC}}(0)D_{\mathrm{int}}$	0.06	0.09	0.06	0.16
D_{int}	1.0	1.0 (∼ 0.85)	0.8 (∼ 1.2)	10.0 (∼ 9.0)
$S_{\mathrm{CC}}(0)D^{Darken}_{\mathrm{int}}$	0.07	0.11	0.08	0.11

the time correlation functions of the longitudinal components of the partial currents (AL and BT), $C^L_{ij}(q,\omega)$, so that $C^L_{ij}(q,\omega) = S_{ij}(q,\omega)\omega^2/q^2$.

We will consider below these longitudinal current correlation functions, which can be helpful in order to discern longitudinal modes not directly visible in $S_{ij}(q,\omega)$, as well as the transverse ones, $C^T_{ij}(q,\omega)$, which provide additional information about collective dynamics in the system associated to the possible propagation of shear waves and enable the calculation of the shear viscosity of the liquid.

Starting from the atomic positions and velocities obtained from the simulations we have evaluated the partial densities and partial currents (longitudinal and transverse components) according to their microscopic definition [34], and from them we have calculated the corresponding time correlation functions and finally their Fourier transforms numerically after applying a window function to alleviate the numerical inaccuracies that typically occur at long times (see appendix B of [56]).

Fig. 6 shows, for some q-values, the calculated partial intermediate scattering functions, $F_{ij}(q,t)$, obtained for $x_{\mathrm{Li}} = 0.17, 0.50$ and 0.80, at similar q-values. At small q's the partials $F_{\mathrm{LiLi}}(q,t), F_{\mathrm{PbPb}}(q,t)$ and $F_{\mathrm{LiPb}}(q,t)$ are dominated by diffusive contributions which impose a slow decay and conceal the oscillations associated with the propagating density fluctuations. Nevertheless, for $x_{\mathrm{Li}} = 0.80$ the decay is distinctly faster and the oscillations are more visible. The BT partial $F_{\mathrm{NN}}(q,t)$ shows a behavior qualitatively similar to that of the AL partials.

The existence of propagating density fluctuations can also be revealed by the presence, within some q-range, of side peaks/shoulders in the partial dynamic structure factors $S_{ij}(q,\omega)$. Fig. 7 depicts our calculated $S_{\mathrm{LiLi}}(q,\omega), S_{\mathrm{PbPb}}(q,\omega)$ and $S_{\mathrm{NN}}(q,\omega)$ at different concentrations and their respective smallest attainable q-value, namely q_{min}. Notice that $S_{\mathrm{NN}}(q = q_{\mathrm{min}},\omega)$ exhibits a shape similar to the hydrodynamic Rayleigh-Brillouin triplet, which for a binary system includes sound propagation contributions in the side peaks and contributions from thermal diffusion and also from interdiffusion in the central line. Adiabatic sound velocities have been estimated from the position of the Brillouin peak in $S_{\mathrm{NN}}(q_{\mathrm{min}},\omega)$, denoted as $\omega_B(q_{\mathrm{min}})$, as $c_s \approx \omega_B(q_{\mathrm{min}})/q_{\mathrm{min}}$. The values we have obtained for $x_{\mathrm{Li}} = 0.17, 0.50, 0.62$ and 0.80 are $c_s \approx$ 1500, 1350, 1600 and 1700 ± 150 m/s, respectively. Comparison with experiment can only be performed for $x_{\mathrm{Li}} = 0.17$ and 0.80, where measurements of the hydrodynamic sound velocity yielded ≈ 1720 m/s [57] and ≈ 2000 m/s [15], respectively. Side peaks/shoulders in $S_{\mathrm{NN}}(q,\omega)$ appear also at higher wavevectors, and the q-range of their appearance has a weak concentration dependence. So, whereas for $x_{\mathrm{Li}} = 0.17$ the calculated $S_{\mathrm{NN}}(q,\omega)$ display side peaks/shoulders up to $q \approx 1.1$ Å^{-1}, this range slightly increases with increasing x_{Li} so that when $x_{\mathrm{Li}} = 0.80$ side peaks/shoulders are found up to $q \approx 1.3$ Å^{-1}.

The $S_{\mathrm{PbPb}}(q,\omega)$ follow a similar trend. As for the $S_{\mathrm{LiLi}}(q,\omega)$, we observe the appearance of small amplitude, but clearly discernible, side peaks/shoulders at frequencies much higher than those shown in Fig. 7, for q-values up to $q \approx 1.3$ Å^{-1} in the case of $x_{\mathrm{Li}} = 0.17$, and

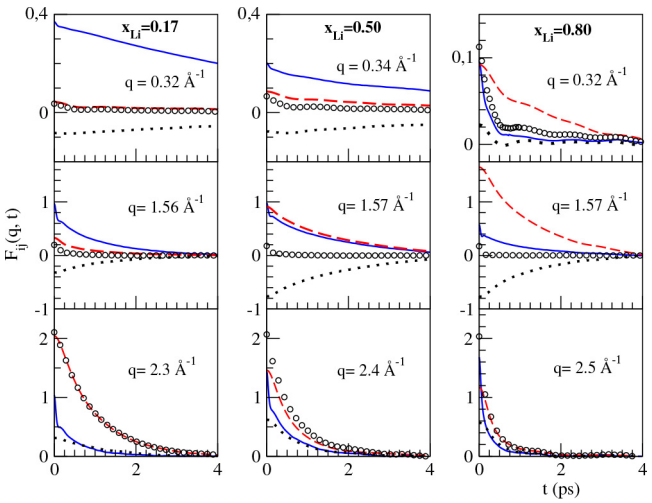

Fig. 6. Partial intermediate scattering functions, $F_{ij}(q,t)$, for the liquid Li_xPb_{1-x} alloy at three concentrations. The solid blue line corresponds to $F_{\mathrm{LiLi}}(q,t)$, the dashed red line to $F_{\mathrm{PbPb}}(q,t)$, and the dotted line is $F_{\mathrm{LiPb}}(q,t)$. Circles denote the BT $F_{\mathrm{NN}}(q,t)$.

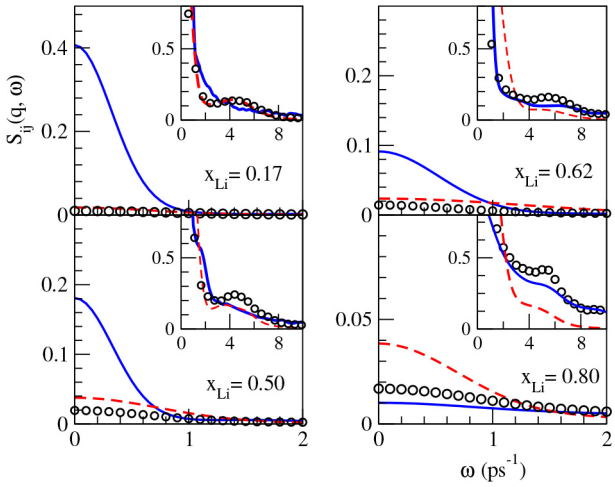

Fig. 7. Partial dynamic structure factors $S_{ij}(q,\omega)$ of the liquid Li_xPb_{1-x} alloy at $x_{\mathrm{Li}} = 0.17, 0.50, 0.62$ and 0.80 for $q = q_{\mathrm{min}} = 0.32, 0.34, 0.35$ and 0.32 Å^{-1} respectively. Full (blue) line, dashed (red) line and circles correspond to $S_{\mathrm{LiLi}}(q,\omega), S_{\mathrm{PbPb}}(q,\omega)$ and $S_{\mathrm{NN}}(q,\omega)$, respectively. The insets show $10^2 S_{ij}(q,\omega)$.

up to $q \approx 1.4$ Å^{-1} for $x_{Li} = 0.80$. These results obtained for $x_{Li} = 0.80$ are qualitatively similar to those provided by the CMD simulations of Bosse et al. [1,2] which yielded $S_{LiLi}(q,\omega)$ with side peaks up to $q \approx 1.2$ Å^{-1}, although their amplitudes were more marked than the present AIMD ones.

From the positions of the side peaks/shoulders in the $S_{LiLi}(q,\omega)$ and $S_{PbPb}(q,\omega)$, we have evaluated the associated dispersion curves, $\omega_{LiLi}(q)$ and $\omega_{PbPb}(q)$ which are depicted in Fig. 8. For all concentrations we obtain two dispersion branches which are indicative of two processes clearly separated in frequency; moreover, their separation increases with increasing Li concentration. The small-q behaviour of the lower frequency branch, $\omega_{PbPb}(q)$, is qualitatively similar to what has been obtained by other authors through CMD simulations or derived from experimental data. Typically, when approaching the hydrodynamic regime, the associated phase velocity is smaller than the hydrodynamic value but as $q \to 0$ this branch smoothly merges into hydrodynamic sound.

The high-frequency branch shows up only in the Li-Li partials. In the case of $x_{Li} = 0.80$, the calculated high frequency branch is compatible with a phase velocity of ≈ 4500 m/s, which is very similar to the results derived from the INS data of Alvarez et al. [7] whose associated phase velocity was also around 4500 m/s. Interestingly, both values are much smaller than that of 7500 m/s obtained by means of CMD simulations. [2,3] The AIMD phase velocity obtained is not far from the hydrodynamic sound velocity that would correspond to pure liquid Li at the same conditions of density and temperature as those of the alloy, as the RET suggests: we have performed an additional AIMD simulation for such a system and obtained a sound velocity of 4150 m/s.

Notwithstanding the importance of the agreement between experiment and our simulations, it has been the physical nature of these high frequency excitations that has sparked strong controversies. It is not clear whether or not when q diminishes towards the hydrodynamic limit, this high frequency branch undergoes a continuous transition into the hydrodynamic sound mode and merges with it, as the RET proposes, or otherwise, the high frequency mode is really a non-hydrodynamic optic-like mode whose weight on the Li-Li partials decreases with decreasing q and of course vanishes at $q = 0$. This debate has mainly revolved around the liquid $Li_{0.80}Pb_{0.20}$ alloy as this is the composition that has attracted the most attention and where this high frequency branch was first detected. This latter interpretation has been suggested by the authors of the INS measurements [7] and also by several theoretical approaches applied to the data obtained from CMD simulations, such as the viscoelastic theory [4], or the GCM approach [12]. In the present AIMD simulations the smallest attainable q-value is ≈ 0.35 Å^{-1}, which is probably outside the hydrodynamic region, so we anticipate that a definite conclusion concerning the low-q behavior of the high frequency branch will not be possible. However, a viable interpretation can be made by observing the trends in Fig. 8 and the additional data provided by the longitudinal current correlation functions to be discussed below.

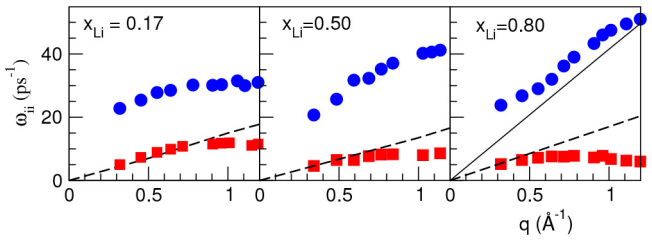

Fig. 8. Dispersion relations, $\omega_{LiLi}(q)$ (full circles) and $\omega_{PbPb}(q)$ (full squares) of the maxima in the partials, $S_{LiLi}(q,\omega)$ and $S_{PbPb}(q,\omega)$ for the liquid Li-Pb alloy at $x_{Li} = 0.17, 0.50$ and 0.80. The slope of the dashed line is the calculated adiabatic sound velocity in the liquid alloy. For $x_{Li} = 0.80$ the slope of full line amounts to a sound velocity of 4150 m/s which corresponds to that of pure Li at the same density and temperature as the alloy, as obtained in an AIMD calculation (see text).

In other AIMD simulation studies of Li-based alloys, namely Li-Ba and Li-Bi [34,58], the evaluation of the respective dispersion relations from the peaks/shoulders of the partial dynamic structure factors yielded also two dispersion branches: a high frequency one associated to Li-Li partials, and a low frequency one. In both alloys when approaching the hydrodynamic region, the corresponding high frequency branch underwent a continuous decrease and merged with the hydrodynamic sound mode from above, while the low frequency brach joined it from below. Nevertheless, the results were also compatible with a scenario where there is not a specific fast-sound mode, but an optic-like non-hydrodynamic mode of higher frequency whose weight on the Li-Li partials decreases as q goes into the hydrodynamic region. The trend obtained in the present study of the Li-Pb alloys, as observed in Fig. 8, points towards a clearer picture than the other Li alloys mentioned before. It does not suggest that the high frequency branch were to (continuously) change its slope and merge into hydrodynamic sound, but rather to tend to a finite non-zero value as q goes to zero, which is the behavior exhibited by optic-like excitations in binary liquids. The case of $x_{Li} = 0.80$ is certainly the most suggestive of this interpretation, but for the other concentrations the picture also looks tenable.

In fact, looking closely at the $S_{LiLi}(q,\omega)$ for small q, and especially in the Li-rich alloys, a shoulder can be observed at a frequency similar to, or slightly larger than, that of the side peak/shoulder corresponding to the Pb-Pb partials (see Fig. 7). Therefore, at least in this region of the phase diagram, it is possible that the true picture is in fact a combination of both theoretical scenarios considered, namely, the Li-Li partials show two modes, the optic-like non hydrodynamic high frequency one, and the extended sound mode with some positive dispersion, whereas the Pb-Pb partials basically exhibit only the extended sound mode, now with a negative dispersion.

As indicated above, the spectra of the current correlation functions, $C^L_{ij}(q,\omega)$, due to the apperance of the factor ω^2, show a depleted contribution coming from the small-ω modes (in particular those of diffusive type), and therefore help to uncover longitudinal modes that are not visible in the partial dynamic structure factors either because of its small weight and/or because they are shielded by the diffusive modes. Fig. 9 shows the AIMD calculated

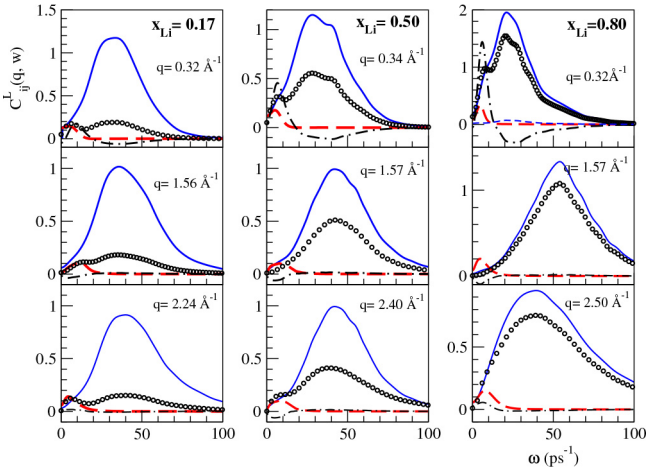

Fig. 9. Partial longitudinal current correlation functions, $C^L_{ij}(q,\omega)$, for the liquid Li_xPb_{1-x} alloy at three concentrations. Full blue line: $C^L_{LiLi}(q,\omega)$, dashed red line: $C^L_{PbPb}(q,\omega)$, dot-dashed line: $C^L_{LiPb}(q,\omega)$ (multiplied by a factor of five for the lowest q-value), and open circles: $C^L_{NN}(q,\omega)$.

$C^L_{ij}(q,\omega)$ for three concentrations and q-values. The $C^L_{\mathrm{LiLi}}(q,\omega)$ and $C^L_{\mathrm{PbPb}}(q,\omega)$ always exhibit only one peak each, located at a high, $\omega^L_{\mathrm{LiLi}}(q)$, frequency, and low, $\omega^L_{\mathrm{PbPb}}(q)$, one, respectively. The $C^L_{\mathrm{NN}}(q,\omega)$ may however display two peaks for some q-ranges and concentrations. In Fig. 9 the cross term has been enhanced multiplying it by a factor of five for $q = q_{\mathrm{min}}$, in order to better observe its behavior. It is seen that the $C^L_{\mathrm{LiPb}}(q)$ also show extrema, that can be of positive or negative sign. It is interesting to note that for these small q values the positive peak in $C^L_{\mathrm{LiPb}}(q)$ is located near $\omega^L_{\mathrm{PbPb}}(q)$, and that also near this frequency a shoulder can be observed in the Li-Li partial. This is the behavior expected for an acoustic mode where all the atoms vibrate in phase. On the contrary, the negative peak in $C^L_{\mathrm{LiPb}}(q)$ is located near $\omega^L_{\mathrm{LiLi}}(q)$, and this suggests that this vibration mode is optic-like, with particles of different type oscillating in opposite phase. This gives further support to the interpreation of the high frequency branch that shows up in the Li-Li partials as an optic-like non-hydrodynamic mode, while the low frequency branch, which appears clearly (as peaks) in the Pb-Pb partials, and weakly (as shoulders) in the Li-Li partials, has an acoustic-like nature, i.e., sound propagation.

The longitudinal dispersion relations, $\omega^L_{ij}(q)$, are depicted for three concentrations in Fig. 10, where we have only included the maxima of the functions, and not the shoulders, in order not to overload the figure. First, notice that the $\omega^L_{\mathrm{PbPb}}(q)$ takes smaller values than those of $\omega^L_{\mathrm{LiLi}}(q)$, because of the greater atomic mass of the Pb atoms/ions. For all concentrations, the $\omega^L_{\mathrm{LiLi}}(q)$ and $\omega^L_{\mathrm{PbPb}}(q)$ have just one branch whereas $\omega^L_{\mathrm{NN}}(q)$ exhibits two. The q-variation of the dispersion relations (apart from their low-q behavior, which obviously is linear for the acoustic mode and going to a non-zero value for the optic-like one) is very much influenced by the corresponding partial structure factors. Minima in $\omega^L_{\mathrm{PbPb}}(q)$ roughly coincide with maxima in $S_{\mathrm{PbPb}}(q)$. And a similar argument applies to the $\omega^L_{\mathrm{LiLi}}(q)$ which, for $x_{\mathrm{Li}} = 0.50$ and 0.80, have a clear minimum, whereas for $x_{\mathrm{Li}} = 0.17$ its almost monotonously increasing shape can be related to the weak double-peak structure of the corresponding $S_{\mathrm{LiLi}}(q)$.

The $\omega^L_{\mathrm{NN}}(q)$ dispersion curve has two branches with low and high frequencies. The high frequency branch exists for the whole q-range and practically coincides with the $\omega^L_{\mathrm{LiLi}}(q)$ branch whereas the low frequency one closely follows the $\omega^L_{\mathrm{PbPb}}(q)$ branch. For the concentration $x_{\mathrm{Li}} = 0.17$ the low frequency $\omega^L_{\mathrm{NN}}(q)$ branch exists for the whole q-range, closely follows the $\omega^L_{\mathrm{PbPb}}(q)$ branch and goes to zero as $q \to 0$. However, when $x_{\mathrm{Li}} = 0.50$ and 0.80, the low frequency $\omega^L_{\mathrm{NN}}(q)$ branch exists only in a very narrow q-range.

We have also included in Fig. 10 for $x_{\mathrm{Li}} = 0.80$, the results deduced from the INS experiments by Alvarez et al. [7], which are very close to our simulation data, and the two propagating modes obtained by Anento et al. [4] through the application of the viscoelastic theory to CMD simulations. We recall that the low frequency mode behaved similarly to sound propagation (without the contribution of thermal fluctuations ignored in the viscoelastic approach) while the high frequency mode was identified as non-hydrodynamic optic-like. Despite the fact that the CMD used the approximate pair potential of Jacucci et al. [1] and the present simulations use the much more accurate DFT method to describe the forces, we find a qualitatively similar behavior of the $\omega^L_{ij}(q)$ and those viscoelastic modes.

We end up the study of the collective dynamic properties of the system considering the spectra of the partial transverse current correlation functons, $C^T_{ij}(q,\omega)$, in their AL and BT formulations, and the frequencies where they show peaks, $\omega^T_{ij}(q)$, which are shown in Fig. 11.

In a similar way as in the case of the longitudinal counterparts, we find that for all concentrations, $\omega^T_{\mathrm{LiLi}}(q)$ shows as high-frequency branch, and $\omega^T_{\mathrm{PbPb}}(q)$ displays a low-frequency branch, but now only for q larger than the long-wavelength propagation gap for acoustic transverse excitations, that takes approximate values of 0.9, 0.5 and 0.3 Å^{-1} for $x_{\mathrm{Li}} = 0.17$, 0.50 and 0.80, respectively. $C^T_{\mathrm{NN}}(q,\omega)$, however, always shows a high frequency peak, which is near $\omega^T_{\mathrm{LiLi}}(q)$, and outside the acoustic propagation gap also a low frequency peak, close to $\omega^T_{\mathrm{PbPb}}(q)$, but only in a limited q-range in the case of $x_{\mathrm{Li}} \geqslant 0.50$.

Even though a theoretically correct description of the acoustic transverse dispersion relation near the propagation gap involves a non-analytic expression involving a square root, it has also been shown that for q just above the propagation gap the dispersion is quasilinear [59], so that it can be reasonably well fitted by a linear expression, $\omega^T_{\mathrm{NN}}(q) \sim c_T(q - q_c)$, where q_c is effectively somewhat smaller then the real propagation gap, whereas the slope, c_T, yields an estimate of the velocity of propagation of the shear modes in the alloy. Such a fit has produced values of $c_T \approx 2300 \pm 150$ m/s for $x_{\mathrm{Li}} = 0.17$, $c_T \approx 3270 \pm 150$ m/s for $x_{\mathrm{Li}} = 0.50$, and $c_T \approx 1000 \pm 150$ m/s for $x_{\mathrm{Li}} = 0.80$. For comparison, we mention that in the limiting case of pure liquid Pb at $T = 650$ K we have obtained $c_T \approx 800 \pm 100$ m/s [31]. Notice that in this linear region $\omega^T_{\mathrm{NN}}(q)$ is close to $\omega^T_{\mathrm{PbPb}}(q)$, which suggests that the acoustic shear modes are propagating through the heavier Pb atoms only.

Concerning the optic-like transverse branch we just mention that its long-wavelength limit is comparable to that of the corresponding longitudinal one, as expected for systems where there are no unscreened Coulomb interactions between particles.

We have also evaluated the alloy shear viscosity, η. This magnitude plays an important role in processes such as fluid transport,

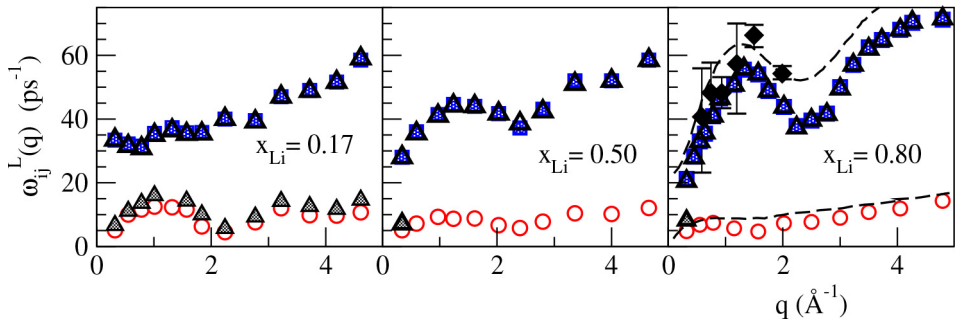

Fig. 10. Longitudinal dispersion relations $\omega^L_{\mathrm{LiLi}}(q)$ (blue squares) $\omega^L_{\mathrm{PbPb}}(q)$ (red circles) and $\omega^L_{\mathrm{NN}}(q)$(open and dashed triangles) for the $\mathrm{Li}_x\mathrm{Pb}_{1-x}$ liquid alloy at several concentrations. The diamonds with error bars are the experimental INS data. The dashed curves stand for the viscoelastic low and high frequency modes obtained in previous CMD calculations [4].

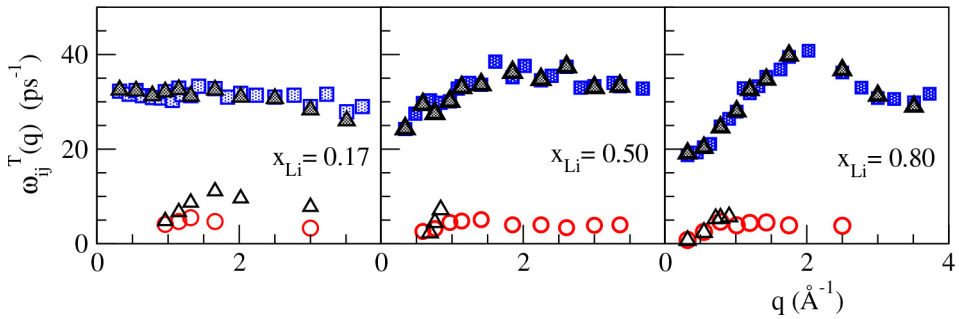

Fig. 11. Transverse dispersion relations $\omega^{T}_{LiLi}(q)$ (open squares), $\omega^{T}_{PbPb}(q)$ (open circles) and number-number, $\omega^{T}_{NN}(q)$ (full and open triangles) for the liquid Li_xPb_{1-x} alloy at $x_{Li} = 0.17$ 0.50 and 0.80.

solidification or reaction kinetics; moreover, experimental measurements are usually problematic so it is important to provide estimates obtained by other methods. For this calculation we used the total transverse current correlation function $C^{T}_{tt}(q,t) = \langle j^{T}_{t}(q,t)\, j^{T\,*}_{t}(q,0)\rangle$ where $j^{T}_{t}(q,t) = x_1^{1/2} m_1 j^{T}_{1}(q,t) + x_2^{1/2} m_2 j^{T}_{2}(q,t)$ is the total transverse current, and more details can be found in [58,60,61].

As a general trend, the shear viscosity of a liquid alloy shows a concentration dependence that is linked to its ordering tendencies. If the alloy has a nearly ideal behaviour, then its η shows either a linear variation with concentration or a small negative deviation from linearity. In case of homocoordinating tendencies the most common behavior is a negative departure from linearity. On the other hand, if the alloy exhibits heterocoordinating tendencies, as in the present case of the liquid Li-Pb alloy, then it is expected that the corresponding η should exhibit positive deviations from linearity. Table 4 and Fig. 12 show our obtained AIMD results along with the experimental data for pure Li and Pb at two temperatures (775 and 1075 K). It is observed that the AIMD results for the shear viscosity at $x_{Li} \geqslant 0.50$ show a positive deviation from linearity, which is greater for $x_{Li} = 0.80$ and smaller for $x_{Li} = 0.50$. This behavior correlates with our previous results about the existence of heterocoordinating tendencies becoming more marked for $x_{Li} = 0.80$. The viscosity of the eutectic alloy does not follow the general trend, as the AIMD result deviates negatively from the linear behavior. Nevertheless, we point out that there is an experimental measurement at this composition, which, as shown in Table 4 and Fig. 12, is fairly close to the AIMD result.

3.3. Electronic density of states

Fig. 13 shows the calculated electronic density of states (DOS) of the liquid $Li_x\ Pb_{1-x}$ alloy for some concentrations and we have also plotted the total DOS of liquid Pb at 650 K obtained by the same AIMD method [31]. Similarly to what we found for liquid Pb, we obtain that the valence electrons are distributed into two bands which are separated by an energy gap that widens with increasing x_{Li} concentration.

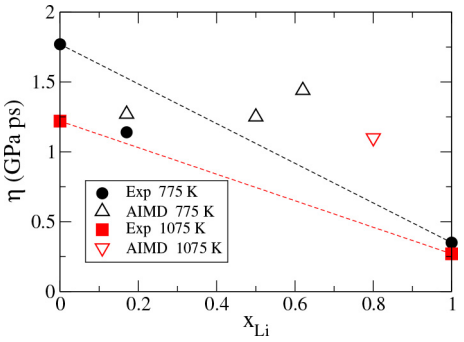

Fig. 12. Viscosity of the liquid Li_xPb_{1-x} alloy at several temperatures and concentrations. The dashed lines correspond to a linear variation with concentration between the experimental liquid Li and Pb values.

The lowest energy band has a predominant *s*-character as it basically contains the 6*s* states of the Pb atom and it gets narrower with increasing Li concentration. In fact, when the Li concentration increases from 0.17 to 0.62, the number of states in this band decreases by a factor of two but this evolution is more intense when approaching the x_{Li}=0.80 as the number of states has been decreased by a factor of four. This evolution is enhanced by the fact that at this concentration there are no PbPb nearest neighbors and therefore there is a negligible overlap of the Pb 6*s* states leading to a very narrow band in the alloy. On the other hand, the highest energy band has a strong *p*-character due to the Pb 6*p* states along with the contribution from the Li 2*s* states. The energy gap between both bands increases with Li concentration and varies in the range $\sim 2.0 - 4.0$ eV. Given the Pb character of the low-lying band and the fact that pure Li is metallic, it is expected that upon further increase in x_{Li} the first band will gradually disappear and a single metallic-like band will be developed. It should also be noted that the electronic behavior of the liquid $Li_x\ Pb_{1-x}$ alloy is quite different from that obtained for a simple liquid metal such as liquid Al, whose electronic DOS is quite close to the free-electron curve [61]. Finally, starting from pure Pb we can observe that upon the

Table 4
Calculated values of the shear viscosity η (in GPa ps) for the liquid Li_xPb_{1-x} alloy at the thermodynamic states given in Table 1. The experimental data for the pure cases were taken from [62] whereas that for the $x_{Li} = 0.17$ was taken from [63].

x_{Li}	T (K)	η	η_{exp}
0	775, 1075		1.77, 1.22 ($\pm$ 0.10)
0.17	775	1.27 $\pm$ 0.15	1.14
0.50	775	1.25 $\pm$ 0.10	
0.62	775	1.44 $\pm$ 0.10	
0.80	1075	1.10 $\pm$ 0.15	
1	775, 1075		0.35, 0.27 ($\pm$ 0.05)

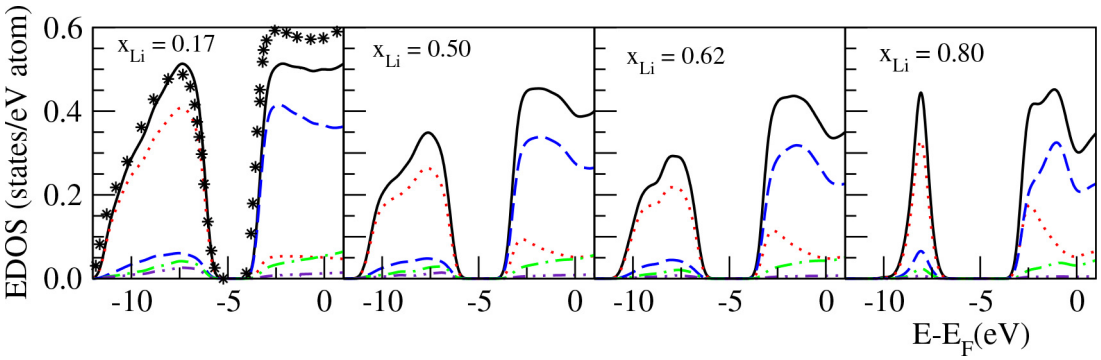

Fig. 13. Calculated total DOS (full black line) for the liquid Li_xPb_{1-x} alloy at x_{Li} = 0.17, 0.50, 0.62 and 0.80. It is also plotted the decomposition of the total DOS into the *s* (dotted line), *p* (dashed line), *d* (dot-dashed line) and *f* (double dotted-dashed line) channels. The stars correspond to the total DOS of liquid Pb at 650 K.

addition of Li, the DOS develops a pseudogap at the Fermi energy, shallow for $x_{Li} = 0.17$ but with an increasing depth for larger Li concentrations, attaining the largest depth at $x_{Li} = 0.80$. This behavior correlates with the maximum of the resistivity at this concentration as measured experimentally [17].

4. Conclusions

This paper reports an AIMD simulation study of several static, dynamic and electronic properties of the liquid Li_xPb_{1-x} alloy at four concentrations.

Concerning the structural properties, the calculated total static structure factors, $S_T(q)$, provide for all concentrations a very good description of the experimental ones; this is remarkable given the strong concentration dependence of the experimental data. The study of the atomic arrangements in the alloys, reveals heterocoordinating tendencies which become very strong at $Li_{0.80}Pb_{0.20}$, where qualitative changes occur with respect to the other concentrations. In fact a polyhedral arrangement, with $Li_{11}Pb$ structures as most abundant, has been found to describe properly the structure at this concentration, in particular discarding completely the existence of Li_4Pb units in the liquid.

Comparison of self- and inter-diffusion coefficients with experiment leads to a good qualitative agreement with the available experimental data, in particular the large increase over Darken's approximation for the interdiffusion coefficient at $x_{Li} = 0.80$, that we relate to the polyhedral structure.

As regards the collective dynamics, several magnitudes has been calculated. The partial dynamic structure factors $S_{LiLi}(q,\omega)$ and $S_{PbPb}(q,\omega)$ exhibit clear side peaks or shoulders over some limited q ranges. The associated dispersion curves, $\omega_{LiLi}(q)$ and $\omega_{PbPb}(q)$ show two distinct dispersion branches whose frequency separation increases with increasing Li concentration. The latter one has an associated phase velocity that in the hydrodynamic limit merges with the hydrodynamic sound from below. On the other hand, the high frequency branch has a trend that suggests optic-like type excitations, an interpretation that is reinforced by the behavior of the Li-Pb longitudinal current correlation function.

We have calculated the alloy shear viscosity by exploiting its conection with the hydrodynamic limit of the total transverse current correlation function. The results show a very good agreement with the available experimental data at the eutectic composition, and correlates with the heterocoordination tendencies at the other concentrations, where no experimental data are available, by exhibiting values larger than those corresponding to a linear variation with concentration.

The calculated electronic DOS curves show that the valence electrons are distributed into two bands separated by an energy gap. One band is basically Pb-*s*-like whereas the other is mainly and Pb-*p*-like, with addition of Li-*s*-like states. The DOS curves clearly point to a metallic behaviour in the alloy but depart from the free-electron curve, and the pseudogap that appears at the Fermi energy correlates with the observed resistivity of the alloy.

These results provide a comprehensive information on the structural, dynamic and electronic properties of the liquid Li_xPb_{1-x} alloy. We expect that this information will contribute towards a better understanding of liquid alloys with fast and slow sound modes.

CRediT authorship contribution statement

M.M.G. Alemany: Methodology, Software, Resources, Investigation, Funding acquisition, Writing – review & editing. **Jaime Souto-Casares:** Methodology, Investigation, Data curation. **Luis E. González:** Software, Investigation, Funding acquisition, Writing – review & editing. **David J. González:** Conceptualization, Supervision, Investigation, Writing – original draft.

Declaration of Competing Interest

The authors declare that they have no known competing financial interests or personal relationships that could have appeared to influence the work reported in this paper.

Acknowledgments

This work was supported by the Spanish Ministry of Economy and Competitiveness in conjunction with the European Regional Development Fund (Project PGC2018-093745-B-I00) and by Xunta de Galicia (GRC ED431C 2020/10). Facilities provided by the Galician Supercomputing Centre (CESGA) are also acknowledged.

References

[1] G. Jacucci, M. Ronchetti, W. Schirmacher, Computer simulation of the liquid Li_4Pb alloy, J. Phys. Colloques 46 (1984) C8–385.
[2] J. Bosse, G. Jacucci, M. Ronchetti, W. Schirmacher, Fast sound in two-component liquids, Phys. Rev. Lett. 57 (1986) 3277.
[3] R. Fernandez-Perea, M. Alvarez, F.J. Bermejo, P. Verkerk, B. Roessli, E. Enciso, Collective ionic dynamics in a molten binary alloy, Phys. Rev. E 58 (1998) 4568.
[4] N. Anento, L.E. González, D.J. González, Y. Chushak, A. Baumketner, Viscoelastic model for the dynamic structure factors of binary systems, Phys. Rev. E 70 (2004) 041201.
[5] P.R. Gartell-Mills, R.L. McGreevy, W. van der Lugt, C. van der Marel, Inelastic neutron scattering studies of molten NaCs alloys, J. Phys. F: Metal Phys. 17 (1987) 2353.
[6] P.H.K. de Jong, P. Verkerk, C.F. de Vroege, L.A. de Graaf, W.S. Howells, S.M. Bennington, Observation of fast sound in liquid Li_4Tl and liquid Li_4Pb by inelastic neutron scattering, J. Phys.: Condens. 6 (Matter 1994,) L681.
[7] M. Alvarez, F.J. Bermejo, P. Verkerk, B. Roessli, High-Frequency Dynamics in a Molten Binary Alloy, Phys. Rev. Lett. 80 (1998) 2141.

[8] L.E. Bove, F. Formisano, E. Guarini, A. Ivanov, C. Petrillo, F. Sacchetti, Evidence for the coexistence of two density fluctuation modes in molten Li_30Bi_{70} as probed by neutron scattering, Europhys. Letters 79 (2007) 16002.

[9] A. Campa, E.G.D. Cohen, Fast sound in binary fluid mixtures, Phys. Rev. A 41 (1990) 5451;
P. Westerhuijs, W. Montfrooij, L.A. de Graaf, I.M. de Schepper, Fast and slow sound in a dense gas mixture of helium and neon, Phys. Rev. A 45 (1992) 3749.

[10] R.L. McGreevy, E.W.J. Mitchell, F.M.A. Margaca, Inelastic neutron scattering studies of the dynamics of molten alkali halides, J. Phys. C: Solid State Phys. 17 (1984) 775.

[11] T. Bryk, I. Mryglod, Collective dynamics in binary liquids: spectra dependence on mass ratio, J. Phys.: Condens. Matter 17 (2005) 413;
T. Bryk, J.-F. Wax, Collective dynamics in a disparate mass molten alloy Li_4Tl: Analysis within the approach of generalized collective modes, Phys. Rev. B 80 (2009) 184206.

[12] T. Bryk, I. Mryglod, Collective excitations and generalized transport coefficients in a molten metallic alloy Li_4Pb, Condens. Matter Phys. 7 (2004) 285.

[13] M.-L. Saboungi, J. Marr, M. Blander, Thermodynamic properties of a quasi-ionic alloy from electromotive force measurements: The Li-Pb system, J. Chem. Phys. 68 (1978) 1375.

[14] W. Becker, G. Schwitzgebel, H. Ruppersberg, Thermodynamic Investigations of Liquid Li-Pb and Li-Ag-Alloys - A Comparative Study, Z. Metallkde. 72 (1981) 186.

[15] H. Ruppersberg, W. Speicher, Density and Compressibility of Liquid Li-Pb Alloys, Z. Naturforsch. A 31 (1976) 47;
J. Saar, H. Ruppersberg, Calculation of $C_p(T)$ for liquid Li/Pb alloys from experimental $\rho(T)$ and $(\delta\rho/\delta T)_s$ data, J. Phys. F: Metal Phys. 17 (1987) 305.

[16] R.A. Khairulin, S.V. Stankus, R.N. Abdullaev, Interdiffusion in lithium-lead melts, Thermophys. Aeromech. 24 (2017) 773.

[17] V. Nguyen, J.E. Enderby, The electronic structure of lithium-based liquid semiconducting alloys, Phil. Mag. 35 (1977) 1013.

[18] A.B. Bhatia, R.N. Singh, Phys. Lett. 78A (1980) 460.

[19] K. Hoshino, W.H. Young, Entropy of mixing of compound forming liquid binary alloys, J. Phys. F: Met. Phys. 10 (1980) 1365.

[20] K. Hoshino, W.H. Young, On the electrical resistivity of the liquid Li-Pb alloy, J. Phys. F: Met. Phys. 10 (1980) L193.

[21] K. Hoshino, Structure of multi-component hard-sphere mixtures- application to the liquid Li-Pb alloy, J. Phys. F: Met. Phys. 13 (1983) 1981.

[22] M. Soltwisch, D. Quitman, H. Ruppersberg, J.B. Suck, Dynamics of concentration fluctuations in a heterocoordinated binary liquid alloy, Phys. Rev. B 28 (1983) 5583.

[23] H. Ruppersberg, H. Egger, Short-range order in liquid Li-Pb alloys, J. Chem. Phys. 63 (1975) 4095.

[24] H. Ruppersberg, H. Reiter, Chemical short-range order in liquid LiPb alloys, J. Phys. F: Metal Phys. 12 (1982) 1311.

[25] M. Soltwisch, D. Quitman, H. Ruppersberg, J.B. Suck, Dynamical structure factor of concentration fluctuations $S_{cc}(Q,\omega)$ measured in the heterocoordinated liquid alloy $Li_{0.8}Pb_{0.2}$, Phys. Lett. A 86 (1981) 241.

[26] A. Fraile, S. Cuesta-López, A. Caro, D. Schwen, J.M. Perlado, Interatomic potential for the compound-forming Li-Pb liquid alloy, J. Nucl. Mater. 448 (2014) 103.

[27] D.K. Belashchenko, Inclusion of the Coulomb Interaction in the Embedded-Atom Model: Lithium-Lead System, High Temp. 57 (2019) 848.

[28] Y. Senda, F. Shimojo, K. Hoshino, Ionic structure and the electronic states of liquid Li-Pb alloys obtained from ab initio molecular dynamics simulations, J. Phys.: Condens. Matter 12 (2000) 6101.

[29] P. Norajitra, L. Bühler, U. Fischer, S. Malang, G. Reimann, H. Schnauder, The EU advanced dual coolant blanket concept, Fusion Eng. Des. 61–62 (2002) 449;
C.P.C. Wong, S. Malang, M. Sawan, M. Dagher, S. Smolentsev, B. Merrill, M. Youssef, S. Reyes, D.K. Sze, N.B. Morley, S. Sharafat, P. Calderoni, G. Sviatoslavsky, R. Kurtz, P. Fogarty, S. Zinkle, M. Abdou, An overview of dual coolant Pb-17Li breeder first wall and blanket concept development for the US ITER-TBM design, Fusion Eng. Des. 81 (2006) 461.

[30] L. Kronik, A. Makmal, M.L. Tiago, M.M.G. Alemany, M. Jain, X.Y. Huang, Y. Saad, J.R. Chelikowsky, PARSEC - the pseudopotential algorithm for real-space electronic structure calculations: recent advances and novel applications to nano-structures, Phys. Status Solidi B 243 (2006) 1063.

[31] M.M.G. Alemany, R.C. Longo, L.J. Gallego, D.J. González, L.E. González, M.L. Tiago, J.R. Chelikowsky, Ab initio molecular dynamics simulations of the static, dynamic, and electronic properties of liquid Pb using real-space pseudopotentials, Phys. Rev. B 76 (2007) 214203.

[32] J. Souto, M.M.G. Alemany, L.J. Gallego, L.E. González, D.J. González, Ab initio molecular dynamics study of the static, dynamic, and electronic properties of liquid Bi near melting using real-space pseudopotentials, Phys. Rev. B 81 (2010) 134201.

[33] K.H. Khoo, M. Kim, G. Schofield, J.R. Chelikowsky, Ab initio molecular dynamics simulations using a Chebyshev-filtered subspace iteration technique, Phys. Rev. B 82 (2010) 064201.

[34] J. Souto, M.M.G. Alemany, L.J. Gallego, L.E. González, D.J. González, Static structure, microscopic dynamics and electronic properties of the liquid Bi-Pb alloy. An ab initio molecular dynamics study, J. Nucl. Mater. 411 (2011) 163;
J. Souto, M.M.G. Alemany, L.J. Gallego, L.E. González, D.J. González, Static structure, microscopic dynamics and electronic properties of the liquid Bi-Li alloy. An ab initio molecular dynamics study, Modelling Simul. Mater. Sci. Eng. 21 (2013) 075006.

[35] M. Kim, K.H. Khoo, J.R. Chelikowsky, Simulating liquid and amorphous silicon dioxide using real-space pseudopotentials, Phys. Rev. B 86 (2012) 054104.

[36] P. Hohenberg, W. Kohn, Inhomogeneous Electron Gas, Phys. Rev. 136 (1964) B864.

[37] W. Kohn, L.J. Sham, Self-Consistent Equations Including Exchange and Correlation Effects, Phys. Rev. 140 (1965) A1133.

[38] M.M.G. Alemany, M. Jain, L. Kronik, J.R. Chelikowsky, Real-space pseudopotential method for computing the electronic properties of periodic systems, Phys. Rev. B 69 (2004) 075101;
M.M.G. Alemany, M. Jain, M.L. Tiago, Y. Zhou, Y. Saad, J.R. Chelikowsky, Efficient first-principles calculations of the electronic structure of periodic systems, Comput. Phys. Comm. 177 (2007) 339.

[39] N. Troullier, J.L. Martins, Efficient pseudopotentials for plane-wave calculations, Phys. Rev. B 43 (1991) 1993.

[40] L. Kleinman, D.M. Bylander, Efficacious Form for Model Pseudopotentials, Phys. Rev. Lett. 48 (1982) 1425.

[41] D.M. Ceperley, B.J. Alder, Ground State of the Electron Gas by a Stochastic Method, Phys. Rev. Lett. 45 (1980) 566.

[42] J.P. Perdew, A. Zunger, Self-interaction correction to density-functional approximations for many-electron systems, Phys. Rev. B 23 (1981) 5048.

[43] D. Beeman, Some multistep methods for use in molecular dynamics calculations, J. Comput. Phys. 20 (1976) 130.

[44] H. Hellmann, Einführung in die Quantenchemie, Deuticke, Leipzig, 1937; R.P. Feynman, Forces in Molecules, Phys. Rev. 56 (1939) 340.

[45] G.R. Goward, N.J. Taylor, D.C.S. Souza, L.F. Nazar, The true crystal structure of $Li_{17}M_4$ (M=Ge, Sn, Pb) - revised from $Li_{22}M_5$, J. Alloys Comp. 329 (2001) 82.

[46] Y. Tsuji, W. Hashimoto, K. Yoshizawa, Lithium-Richest Phase of Lithium Tetrelides $Li_{17}Tt_4$ (Tt = Si, Ge, Sn, and Pb) as an Electride, Bull. Chem. Soc. Jpn. 92 (2019) 1154.

[47] S. Kohara, J. Akola, L. Patrikeev, M. Ropo, K. Ohara, M. Itou, A. Fujiwara, J. Yahiro, J.T. Okada, T. Ishikawa, A. Mizuno, A. Masuno, Y. Watanabe, T. Usuki, Atomic and electronic structures of an extremely fragile liquid, Nat. Commun. 5 (2014) 5892.

[48] R.L. McGreevy, A. Baranyai, I. Ruff, A Less Arbitrary Determination of Coordination Numbers in Disordered Systems, Phys. Chem. Liq. 16 (1986) 47.

[49] C.N.J. Wagner, H. Ruppersberg, Application of Nuclear Techniques to the Studies of Amorphous Metals, ed. U. Gonser, Atomic Energy Review, Supplement 1, 101, 1981.

[50] U. Balucani, M. Zoppi, Dynamics of the Liquid State, Clarendon, Oxford, 1994.

[51] J.P. Hansen, I.R. McDonald, Theory of Simple Liquids, Academic Press, New York, 1986.

[52] J.P. Boon, S. Yip, Molecular Hydrodynamics, McGraw-Hill, New York, 1980.

[53] N.H. March, M.P. Tosi, Atomic Dynamics in Liquids, Dover, New York, 1991.

[54] G.E. Bacon, Neutron Diffraction, Clarendon, Oxford, 1975.

[55] J. Trullás, J.A. Padró, Diffusion in multicomponent liquids: a new set of collective velocity correlation funcions and difusion coefficients, J. Chem. Phys. 99 (1993) 3983;
J. Trullás, J.A. Padró, Self- and cross-velocity correlation functions and diffusion coefficients in liquids: A molecular dynamics study of binary mixtures of soft spheres, Phys. Rev. E 50 (1994) 1162.

[56] M. Marqués, L.E. González, D.J. González, Ab initio study of the structure and dynamics of bulk liquid Fe, Phys. Rev. B 92 (2015) 134203.

[57] Y. Ueki, M. Hirabayashi, T. Kunugi, T. Yokomine, K. Ara, Acoustic Properties of Pb-17Li Alloy for Ultrasonic Doppler Velocimetry, Fusion Sci. Technol. 56 (2009) 846.

[58] D.J. González, L.E. González, J.M. López, M.J. Stott, Collective modes in liquid binary alloys. An ab initio molecular dynamics study of the LiMg and LiBa alloys, J. Phys.: Condens. 17 (Matter 2005,) 1429.

[59] B.G. del Rio, L.E. González, Orbital free ab initio simulations of liquid alkaline earth metals: from pseudopotential construction to structural and dynamic properties, J. Phys.: Condens. 28 (Matter 2014,) 4651102.

[60] J. Blanco, D.J. González, L.E. González, J.M. López, M.J. Stott, Collective ionic dynamics in the liquid Na-Cs alloy: An ab initio molecular dynamics study, Phys. Rev E 67 (2003) 041204.

[61] M.M.G. Alemany, L.J. Gallego, D.J. González, Kohn-Sham ab initio molecular dynamics study of liquid Al near melting, Phys. Rev. B 70 (2004) 134206.

[62] M. Shimoji, I. Itami, Atomic Transport in Liquid Metals, Trans Tech, Switzerland, 1986.

[63] B. Schulz, Thermophysical properties of the Li(17)Pb(83) alloy, Fusion Eng. Des. 14 (1991) 199.